Modal approach based on global stereo-correlation for defects measurement in wire-laser additive manufacturing

Khalil Hachem, Yann Quinsat, Christophe Tournier, Nicolas Béraud

Modal approach based on global stereocorrelation for defects measurement in Wire-Laser Additive Manufacturing

Khalil Hachem[a], Yann Quinsat[a], Christophe Tournier[a], and Nicolas Beraud[b]

[a] *Université Paris-Saclay, ENS Paris-Saclay, LURPA, 91190 Gif-sur-Yvette, France*
[b] *Univ. Grenoble Alpes, CNRS, Grenoble INP, G-SCOP, 38000 Grenoble, France*

ABSTRACT

Producing Near Net Shape parts with complex geometries using Wire-Laser Additive Manufacturing often requires a mastered and optimized process. Differences between the constructed and nominal geometries of the manufactured entities demand an in-situ defects measurement to complete the production of the entire part successfully. A contactless measuring system is needed to evaluate geometrical deviations without requiring complex post-processing operations. To overcome this challenge and validate a measuring tool that serves the manufacturing purpose, a global stereocorrelation approach is used to measure defects in wire-laser additively manufactured parts. This method relies on the cameras' self-calibration phase that uses the part substrate's nominal model. Then a modal basis is defined to model and evaluate the surface dimensional and shape defects. Hence, an analysis of the texture obtained in additive manufacturing is conducted to assess whether or not it is sufficient for image correlation and defects measurement. Finally, natural and pattern textures are compared to highlight their influence on the measurement results.

Keywords: Wire-Laser Additive Manufacturing, image correlation, defects measurement, modal basis, texture analysis.

1. INTRODUCTION

A new industrial manufacturing era started with the evolution of Additive Manufacturing (AM). This process entered high levels of industry and production. Its advantage over the subtractive techniques is producing parts with complex internal and external features[1] and repairing damaged parts.[2] Wire-Laser Additive Manufacturing (WLAM) is a branch of AM processes where a stream of metal wire is delivered to a substrate in order to intersect with a concentrated laser energy source at a common focal point, forming a melt pool and depositing material layer by layer. The corresponding machine includes a laser system and an automated wire feed supply unit moved by an operated robot arm. The machine worktable can achieve rotary substratum movement, and some accessory devices, such as gas shielding, are necessary. Additively manufactured parts present different types of defects and deviations from the nominal design. Therefore, on a larger scale, classifications exist for Directed Energy Deposition (DED) processes that include the wire-laser one. According to Liu *et al.*,[3] part quality and defects affecting DED parts can be classified into three categories: geometrical (form and dimensions), morphological (surface texture), and microstructural anomalies. From here, and at both layers and entities level, defects in WLAM can be seen and treated as internal and external. In the following, this paper highlights external defects, more precisely geometrical ones where dimensional and shape deviations can be found.

Complex geometries in AM often require more than one deposition sequence. The part can be built through many stages while changing its position and orientation between phases. From here, differences between the produced and nominal geometries can penalize the whole ongoing and upcoming process. These defects can be seen at the entity level as geometrical positioning and orientation deviations, or at the surface level as material gaps on the final parts, blobs, and zits. All these risk collisions between the effector and the part, in addition to disturbing the additive trajectories and piling up defects through the end of the process. That is why it is necessary to measure these deviations *in-situ* in order to update the additive trajectories with regard to the occurring geometrical defects. A contactless measuring system is mandatory to evaluate geometrical defects

Contact author information: Khalil Hachem, khalil.hachem@ens-paris-saclay.fr, +33 (0)7 69 48 06 48

without requiring complex post-processing operations. It also helps to achieve *in-situ* measurements without interrupting the process or removing the part from its manufacturing environment. Hence, optical signal-based detection with its spatially resolved CCD/CMOS cameras is becoming more popular, especially with the evolution of the image correlation technique.[1] Its capability to provide full-field measurements with a direct evaluation of the part deformation is valuable and efficient in shape measurement.[4] Rebergue *et al.*[5] and Dubreuil[6] achieved *in-situ* measurements during machining using Digital Image Correlation (DIC). In contrast, Dufour[7] used this technique to measure 3D displacement fields with a numerical description of the analyzed surfaces (NURBS).

Modal decomposition, based on free vibrational modes, proved its relevance for form defect analysis and was used in different previous works, having the same objective of identifying and expressing shape deviations of thin parts[8] and medium-sized machined surfaces.[4] More precisely, shape defect is decomposed of several elementary participations, whose sum best fits the observed defects. From here, Etievant *et al.* developed a modal approach for shape defect measurement based on global stereocorrelation.[4] This work includes a self-calibration phase where the measured object is used as a calibration artifact.[9,10] The nominal description of the part is defined as a triangular mesh, and a speckle pattern is projected on the machined surface to texture it. This step is followed by global DIC measurement and defects evaluation using a predefined modal basis. This paper aims to use this approach to measure the shape and dimensional defects of parts produced by the WLAM process. By introducing this technique to the AM context, the surface texture became a new variable that needs to be assessed. Unlike machined surfaces, it's a natural pattern that may influence the image correlation analysis over a Region Of Interest (ROI). From here, a study comparing results obtained with natural and classic projected patterns is critical to know whether the manufactured part texture is enough to exclude any added pattern. Finally, AM surfaces presenting remarkable defects question their use as targets in the self-calibration procedures and shift the attention to well-defined geometries from the manufacturing environment, such as the part's substrate.

This contribution is structured as follows: in Sec. 2, the adopted approach and its measurement principles are presented. Then, the case study with all its phases and results are detailed in Sec. 3. The findings and perspectives of this research work are finally summarized in Sec. 4.

2. MEASUREMENT APPROACH

In this work, the shape defects of an AM part are measured by global stereocorrelation. Therefore, calibrating the cameras is fundamental here, especially in an AM context where the surface texture and geometrical deviations can't be neglected. In addition to the optical measurements, this study uses a modal approach to express the geometric deviations. In this section, the camera model is presented alongside the self-calibration technique. Then, the shape correction method is addressed, and analysis criteria are defined for the texture comparison.

2.1 Camera model and calibration

The pinhole camera model is the most specialized and simplest one. It describes the process of image formation within a camera to express the relationship between the 3D coordinates ($\mathbf{X}$) of a point in space, and its corresponding pixel coordinates ($\mathbf{x}$) in the image plane. A total of six unknowns, 3 rotation parameters, and 3 distances are essential to define the rigid transformation between the space and camera frame. They are referred to as extrinsic parameters. Once in the camera coordinate frame, the point projection in the image plane is defined by the following intrinsic parameters: the focal length expressed in pixels (width and height), the skew factor between the axis of the image plane, and the coordinates of the optical center projection. Finally, image distortions are computed and taken into consideration. Therefore, the calibration of a stereoscopic system (having at least two cameras) is summed up by determining all these parameters for each camera.

Adapting the self-calibration method leads to using the same image for the calibration and the measurement. Hence, this approach requires a mathematical description of the analyzed surface, whether NURBS patches[9] or triangular meshes.[4,10] The main objective is to determine the left and right camera calibration matrices such that the 3D numerical model of the object is best projected on both images. First, the transformation matrices are initially determined by manual projections. Then in the second step, an underlying minimization principle is used. It's based on the gray level conservation (Eq. 1) in the acquired left $f^l(\mathbf{x^l})$ and right $f^r(\mathbf{x^r})$ images.

$$f^l(\mathbf{x^l}) = f^r(\mathbf{x^r}) \tag{1}$$

Hence, over an ROI, global minimization of the correlation residual is executed to determine the optimal solution of the left $[\mathbf{P^l}]$ and right $[\mathbf{P^r}]$ projection matrices (Eq. 2), therefore the stereoscopic system calibration.[4] This Gauss-Newton problem is linearized in Eq. 3 where the image gradient is represented by ∇f.

$$\left([\mathbf{P^l}],[\mathbf{P^r}]\right) = \underset{[\mathbf{P^l}],[\mathbf{P^r}]}{argmin} \sum_{ROI} \left(f^l\left([\mathbf{P^l}](\mathbf{X_0})\right) - f^r\left([\mathbf{P^r}](\mathbf{X_0})\right)\right)^2 \tag{2}$$

$$\tau_{lin} = \sum_{ROI} \left(f^l(\mathbf{x^l}) - f^r(\mathbf{x^r}) + (\nabla f^l.\delta\mathbf{x^l})(\mathbf{x^l}) - (\nabla f^r.\delta\mathbf{x^r})(\mathbf{x^r})\right)^2 \tag{3}$$

A Canon EOS7D camera is used in this research work, and the pinhole model is adapted. The calibration is done separately and intrinsic parameters are found using a calibration target presenting a circular pattern. Radial and tangential distortions are calculated and removed from the taken part images using a Matlab toolbox. In contrast, extrinsic ones are computed using the self-calibration approach adapted by Etievant *et al.*[4] but relying on the substrate instead of the manufactured surface. This change is due to the significant defects present on the AM part. That's why well-defined geometrical features from the part environment are used to ensure proper solution convergence during optimization. Detailed steps and results of this procedure are presented in Sec. 3.

2.2 Shape measurement and correction

Once the calibration is performed, the nominal surface is deformed using a defect database obtained by modal analysis. Hence, the estimate of the modal deformation $\mathbf{X}$ is computed by starting with the nominal position vector $\mathbf{X_0}$ (Eq. 4) and adding to it the corresponding displacement that best expresses the present shape defect. Λ_i are the modal amplitudes associated with the N modes $\mathbf{q_i}$.

$$\mathbf{X} = \mathbf{X_0} + \sum_{i=1}^{N} \Lambda_i.\mathbf{q_i} \tag{4}$$

As shown in Eq. (5), modal amplitudes are determined to minimize the global correlation residuals over an ROI. The problem is linearized in the same way as in Eq. (3). A Gauss-Newton algorithm is implemented where the minimization procedure stops once the corrections to the estimated modal amplitudes are very low. This explains the need for a higher image gradient for faster and better convergence. The modal basis is projected according to the normal of the local surface to highlight displacements induced by shape defects.[4]

$$\{\mathbf{\Lambda_{opt}}\} = \underset{\{\mathbf{\Lambda}\}}{argmin} \sum_{ROI} \left(f^l\left([\mathbf{P^l}](\mathbf{X})\right) - f^r\left([\mathbf{P^r}](\mathbf{X})\right)\right)^2 \tag{5}$$

2.3 Image analysis

Image correlation is an experimental technique for measuring field displacement by matching digital photos of an object. Hence, being in a new manufacturing context and questioning the natural surface capabilities requires finding criteria to qualify the images before the measurements and comparing the different textures.

First, an image gradient (∇f) is a directional change in intensity that characterizes the image's contrast. It is defined by a 2D vector with components given by the derivatives in the horizontal G_x and vertical G_y directions. Moreover, it's a crucial element in the linearized optimization problems of this study. From here, an Average Gradient (AG) is computed (Eq. 6),[11] where $H \times W$ is the size of the image (its height and width expressed in pixels). Hence, a better AG allows better convergence of the correlation residuals. On the other hand, spatial autocorrelation refers to the presence of a spatial variation in the mapped variable. This criterion is computed in Eq. (7), where σ is the standard deviation (STD). The output is the normalized correlation ($-1 < C < 1$); a null value is the perfect case, while $C > 0$ means that adjacent observations have similar data values. This criterion compares the image with itself but with a displacement of pixels (δ) in horizontal and vertical directions. By focusing on the surface of interest, the mapping results inform about the sensitivity to variations. Finally, the case study in the following section lists these criteria's numerical application.

$$AG = \frac{1}{(H-1)(W-1)} \sum_x \sum_y \frac{\sqrt{G_x^2 + G_y^2}}{\sqrt{2}} \tag{6}$$

$$C(\delta) = \frac{\overline{f(\mathbf{x}) f(\mathbf{x}+\delta)} - \overline{f(\mathbf{x})}^2}{\sigma^2(f)} \tag{7}$$

3. CASE STUDY

The presented study is conducted on a WLAM part to validate the use of the modal approach based on global stereocorrelation in the measurement of geometrical defects by comparing these results with another industrial measuring method. The considered part is a $42.7mm \times 42.7mm$ hollow column with a height of 35mm centered on an $80mm \times 80mm \times 20mm$ substrate whose nominal description is defined in a CAD model. Different surface meshes are used during the different steps of the method. Table 1 summarizes the use of each mesh and its visualization. The first two meshes rely on the substrate surfaces, while the third one uses the AM one.

Table 1. Description of the different used meshes.

Mesh Number	**Used for**		
#1	Estimation of initial parameters	Left extrinsic parameters	Fig. 1a
		Right extrinsic parameters	Fig. 1b
#2	Extrinsic calibration		Fig. 1c
#3	Modal basis creation / Defects measurement		Fig. 1d

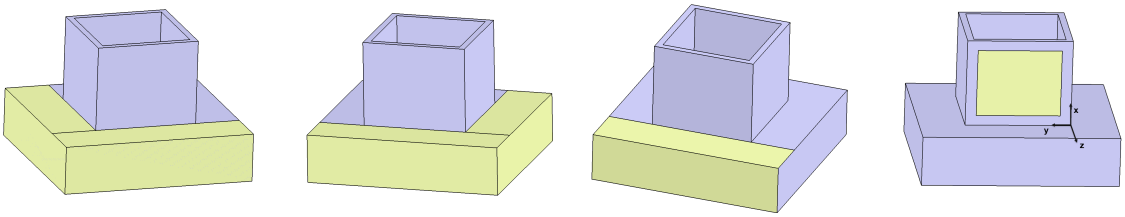

(a) (b) (c) (d)

Figure 1. Surfaces used for the initial parameters estimation (a,b), extrinsic calibration (c) and defects measurement (d).

3.1 Reference measurement

In order to validate the stereocorrelation measurement results, it is essential to estimate the geometrical defects using a reference system, in the present case, a structured light scanning device (Atos Core). This optical system efficiently measures complex shapes,[4] with low uncertainty and an STD shape error of 3 µm. Once the part is measured, a point cloud is obtained and must be processed to extract the geometrical deviations. First, the ATOS Core measurement frame is aligned with the CAD model. The substrate nominal description is used for this point cloud frame realignment. A non-rigid registration algorithm for form defect identification is implemented in the second step. This method, developed by Thiébaut *et al.*,[8] is based on a deformable Iterative Closest Point (ICP) algorithm and a modal approach to express form defects.

A defect basis is defined using the third mesh (Fig. 1d). Since the objective is to evaluate defects along the surface normal (z-axis), these rigid modes can be reduced to 3 to model dimensional deviations. The first mode represents a translation along the z-axis, while the second and third are rotations around the x- and y-axes, respectively. Geometrical deviations of the part were estimated using these 3 modes (Fig. 2a). The results showed important dimensional defects concerning the column position (Mode #1 in Fig. 2c) and inclination (Modes #2-3 in Fig.2c). Then, the rest of the deformable modes are defined as sinusoidal functions,[8] representing shape

defects. A total basis of 25 modes is used, and modes with nearly zero z-components (normal surface direction) have been eliminated from this basis. Figure 2b shows the geometrical defects expressed by the non-rigid body modes of the adapted basis. This estimation is enough to measure dimensional and shape deviations while increasing the modal basis size won't add remarkable variations to the displacement maps. The ATOS Core measurement and defects modeling using the 25 modes basis are used as the reference in the following.

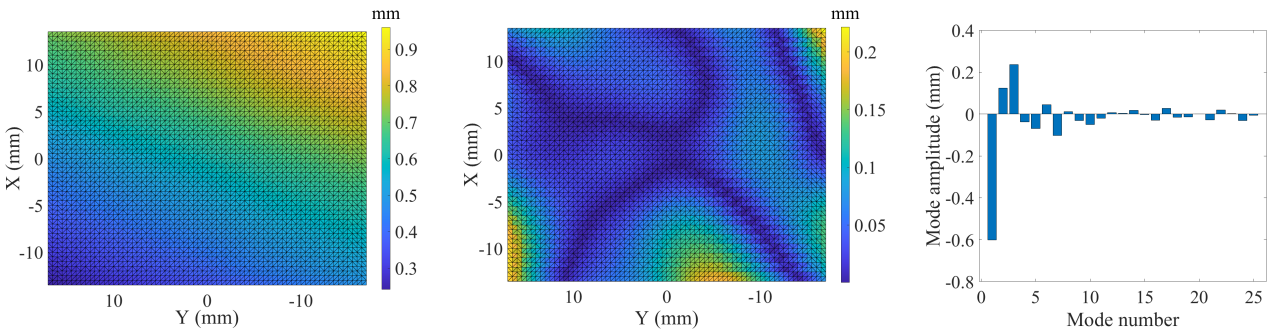

Figure 2. Geometrical defects measured by 3 rigid body modes (a) and the following 22 (b); Modal amplitudes using ATOS Core with a modal basis of 25 modes (c).

3.2 Texture analysis

In the following, three different textures of the AM surface (Fig. 3 a,b,c) are analyzed and compared using the defined criteria in Sec. 2.3. This analysis evaluates each pattern, especially the natural AM surface and what it can provide for the image correlation analysis. It helps also predict and understand measurement results in Sec. 3.3. As shown in Tab. 2, the average gradient increases with a pattern projection on the natural texture, especially the speckle one. In addition to that, a comparison of the three spatial autocorrelation maps (Fig. 3 d,e,f) shows a clear advantage of the speckle pattern projection. This result can also be seen by comparing the computed autocorrelation Root Mean Square (RMS), where the third texture presents better results with a value closer to zero (0.051). Self-image comparison with pixels displacements using the regular and well-defined circular pattern leads to similar and contrasting data values, which explains the yellow-blue pattern in Fig. 2e.

Table 2. Image correlation criteria comparison for different textures.

	Natural texture	**Circle Pattern**	**Speckle Pattern**
AG $(1/\text{Pixels}^2)$	0.055	0.071	0.093
Autocorrelation RMS	0.072	0.210	0.051

3.3 Modal stereocorrelation measurements

First, and before introducing the measurement results, camera calibration is essential here. After fixing the Canon EOS7D intrinsic parameters, left and right pictures of the AM part are used to compute the extrinsic ones. This manufactured column presents remarkable defects as shown in Fig. 2. That's why the extrinsic calibration steps are based on a powdered substrate with a projected circle pattern. In some cases, the substrate geometry is deformed during additive manufacturing due to higher generated heat, mainly while producing solid instead of hollow parts. In the following procedure, the shape of the substrate is considered geometrically perfect. In the first step, the nominal 3D meshes of the substrate surfaces, highlighted in Fig. 1(a,b), are projected on the left and right part images. Then, these meshes are manually aligned by estimating the initial extrinsic parameters. Hence, these previous estimations map the second mesh (Fig. 1c) from its 3D frame to image one. A self-calibration calculation based on the image correlation technique follows. Therefore, extrinsic projection matrices are optimized to minimize correlation residuals (Eq. 2). 60 iterations were needed in order to converge towards the final solutions with the use of a Levenberg-Marquardt regularization.

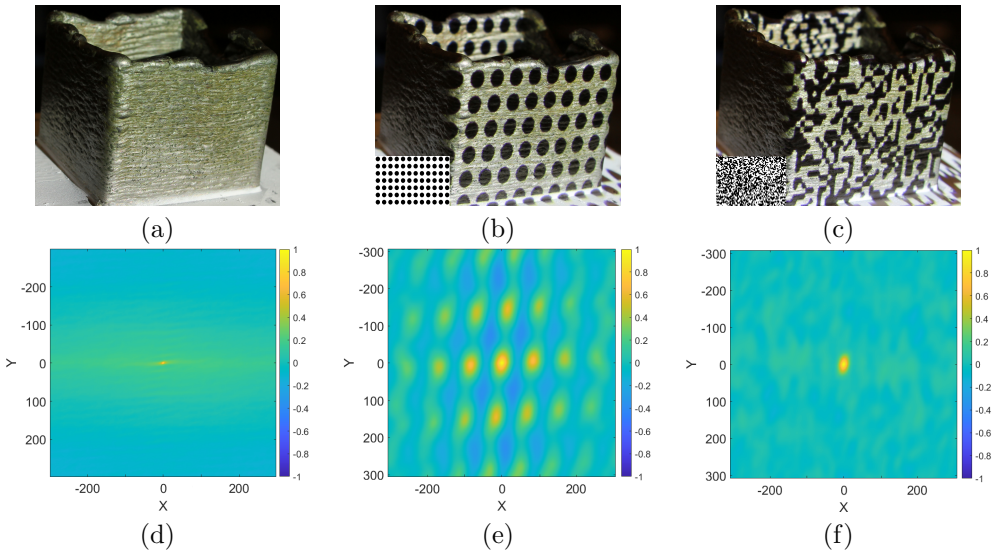

Figure 3. WLAM surface with natural texture (a), circle (b), and speckle (c) pattern projection and their corresponding spatial autocorrelation map (d,e,f).

In the following, stereocorrelation measurements are performed using pair images presenting the three different textures introduced in Sec. 3.2. Therefore, after the optical measurements comes the geometrical defects modeling. The nominal mesh is then deformed using Eq. 4 and the 25 modes basis. At the same time, optimized modal amplitudes are computed to minimize correlation residuals (Eq. 5). The convergence of the correlation residuals is smoother and almost 20 times faster with pattern texture, as shown in Fig. 4. A better convergence validates the importance and influence of a better image gradient. In a second step, these results are compared to the reference one (ATOS Core measurement). A difference map is obtained by computing the difference between the calculated displacements in each measuring method and for each texture. This map can be presented numerically through the RMS of these displacement differences computed at the end of the optimization (Tab. 3). Moreover, having the differences STD and the defects' maximum amplitude, a measurement relative error is calculated. All these results show that stereocorrelation measurements are relevant and close to the reference. Hence, the pattern projection advantage was expected, especially the speckle one. The lower error can be explained by the autocorrelation criterion. In contrast, considering the objective of these defects measurements (updating additive trajectories), the natural texture shows promising results, since in this case, an error of 2.72% is entirely consistent with the requirements of the process.

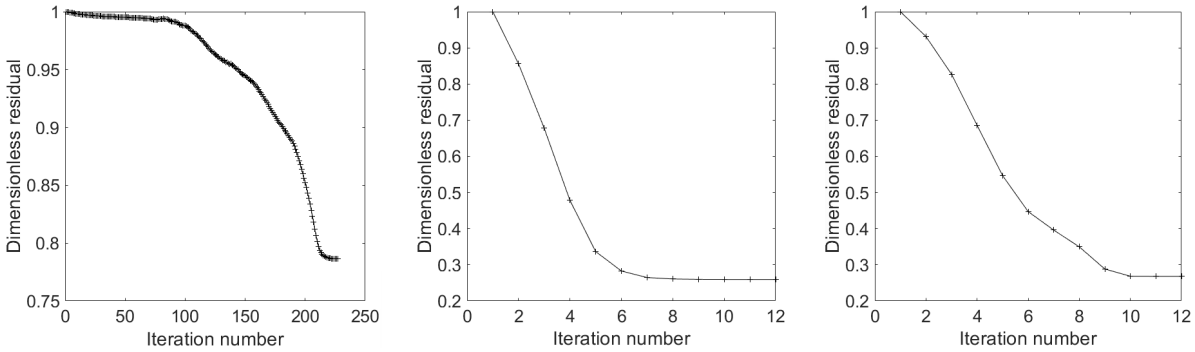

Figure 4. Correlation residuals convergence curves using natural texture (a), circle (b), and speckle (c) patterns projection.

Table 3. Stereocorrelation measurements compared to the reference ones using different textures.

	Natural texture	**Circle Pattern**	**Speckle Pattern**
Differences with ATOS Core (RMS)	$51.53\mu m$	$35.73\mu m$	$26.3\mu m$
Measurements relative error	2.72%	2.22%	1.65%

The purpose of this comparison is to respond to the goal of this paper; determine the influence of these patterns and highlight the promising performance of the natural one. In addition, the results explain the link between the measurements and the criteria presented in Tab. 2, and validate the applicability of this modal stereocorrelation approach in an AM context.

Elements and results from the third texture case are presented next. The pair of images, with speckle pattern projection, used in the stereocorrelation defects measurements is shown in Fig. 5a. Previously, the residuals convergence curve was presented, while Fig. 5(b,c) shows the corresponding map before and after shape correction. These results give clear information about the residuals minimization. Therefore, low and uniform residuals validate the sufficiency of the adapted modal basis in describing the geometrical defects. The shape correction map is visualized separately using the rigid body modes (Fig. 6a), and the 22 that follows (Fig. 6b). Their corresponding modal amplitudes distribution is shown in Fig. 6c.

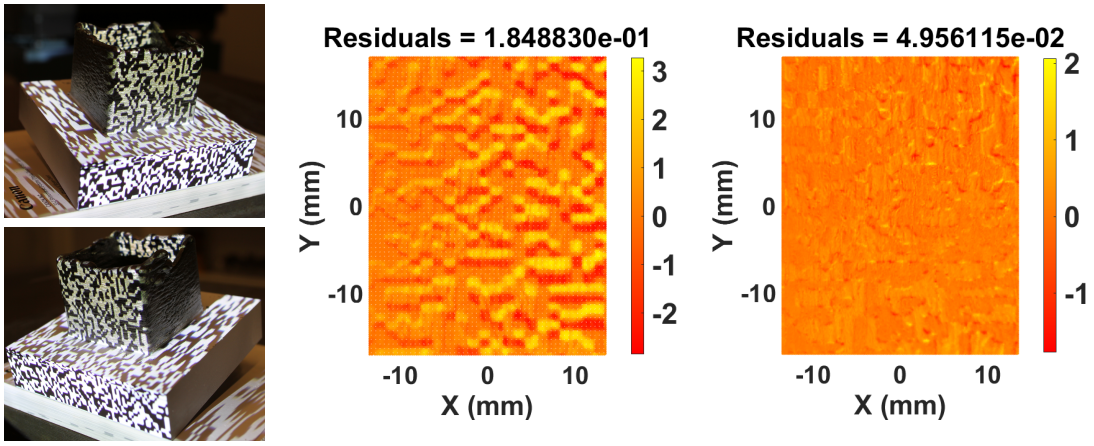

(a) (b) (c)

Figure 5. Pair of images required for the modal stereocorrelation measurement (a); Correlation residuals map (expressed in % of dynamic range) before (b) and after (c) shape correction.

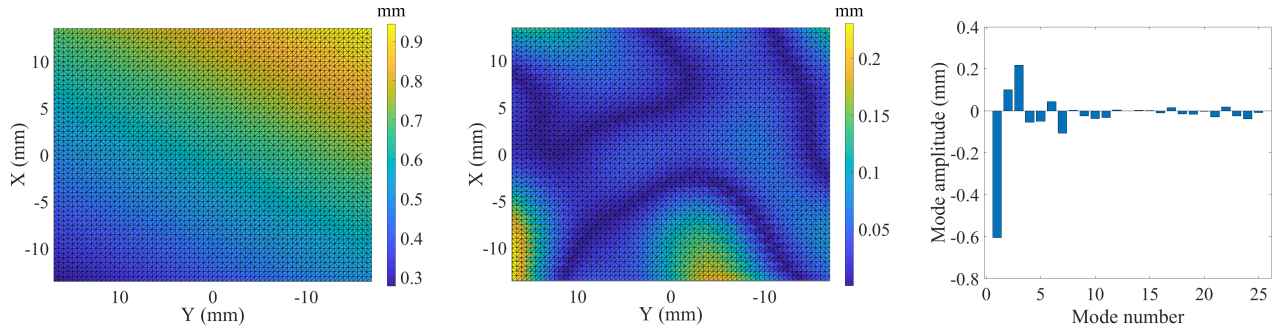

(a) 3 rigid body modes (b) 22 vibrational modes (c) Modal amplitudes

Figure 6. Stereocorrelation measurement results with speckle texture. Geometrical defects (a,b), and modal distribution using a 25 modes defect basis (c).

4. CONCLUSION

This work applies a modal approach based on global stereocorrelation to measure dimensional and shape defects in WLAM part. A Canon EOS7D camera is used and calibrated by determining its intrinsic and extrinsic parameters separately. Intrinsic parameters are found using a calibration target. In contrast, a self-calibration step computes extrinsic ones based on the part substrate instead of the measured surface itself due to its remarkable defects. A modal basis of 25 modes is defined, and the stereocorrelation results are compared to defects measured with a reference system (ATOS Core). A 1.65% error compared to the reference system can validate the adapted measurement tool in this research context. It's also important to highlight the pattern projection influence on the measurement results. This texture presents a higher gradient, leading to faster and better convergence of the correlation residuals optimization. In addition, the results obtained with a projected speckle pattern are closer to those measured by the ATOS Core. In contrast, the natural AM texture presented interesting results and sufficient pattern to achieve the measurements.

In future work, an *in-situ* measuring system based on image correlation (CMOS Cameras) will be placed in the hybrid robot cell. A defect base representative of the geometric defects obtained in WLAM processes will be defined on entities scale. From here, a technological defect database will be built either by experiments on the process parameters and ATOS Core measurements or by a complete numerical approach. Finally, reconstruction algorithms of a model representing the acquired part geometry with its defects will be developed to realign the additive trajectories and optimize the manufacturing process, which is the primary goal of these upcoming works.

ACKNOWLEDGMENTS

The authors gratefully acknowledge the technical support provided by the Paris-Saclay Additive Manufacturing Platform funded by Université Paris-Saclay and École normale supérieure Paris-Saclay through the strategic research initiative program (ANR-11-IDEX-0003-02).

REFERENCES

[1] Chen, X., Kong, F., Fu, Y., Zhao, X., Li, R., Wang, G., and Zhang, H., "A review on wire-arc additive manufacturing: typical defects, detection approaches, and multisensor data fusion-based model," *The International Journal of Advanced Manufacturing Technology* **117**(3-4), 707–727 (2021).

[2] Svetlizky, D., Das, M., Zheng, B., Vyatskikh, A. L., Bose, S., Bandyopadhyay, A., Schoenung, J. M., Lavernia, E. J., and Eliaz, N., "Directed energy deposition (DED) additive manufacturing: Physical characteristics, defects, challenges and applications," *Materials Today* **49**, 271–295 (2021).

[3] Liu, M., Kumar, A., Bukkapatnam, S., and Kuttolamadom, M., "A review of the anomalies in directed energy deposition (DED) processes & potential solutions - part quality & defects," *Procedia Manufacturing* **53**, 507–518 (2021).

[4] Etievant, D., Quinsat, Y., Thiebaut, F., and Hild, F., "A modal approach for shape defect measurement based on global stereocorrelation," *Optics and Lasers in Engineering* **128**, 106030 (2020).

[5] Rebergue, G., Blaysat, B., Chanal, H., and Duc, E., "In-situ measurement of machining part deflection with Digital Image Correlation," *Measurement* **187**, 110301 (2022).

[6] Dubreuil, L., *Mesure In-situ par moyens optiques*, PhD thesis, Université Paris-Saclay (2017).

[7] Dufour, J.-E., *Mesures de forme, de déplacement, et de paramètres mécaniques parstéréo-corrélation d'images isogéométrique*, PhD thesis, Université Paris-Saclay (2015).

[8] Thiébaut, F., Bendjebla, S., Quinsat, Y., and Lartigue, C., "Nonrigid registration for form defect identification of thin parts," *Journal of Computing and Information Science in Engineering* **18**(2), 021012 (2018).

[9] Beaubier, B., Dufour, J.-E., Hild, F., Roux, S., Lavernhe, S., and Lavernhe-Taillard, K., "CAD-based calibration and shape measurement with stereoDIC: Principle and application on test and industrial parts," *Experimental Mechanics* **54**(3), 329–341 (2014).

[10] Dubreuil, L., Dufour, J.-E., Quinsat, Y., and Hild, F., "Mesh-Based Shape Measurements with Stereocorrelation: Principle and First Results," *Experimental Mechanics* **56**(7), 1231–1242 (2016).

[11] Zhao, C., Wang, Z., Li, H., Wu, X., Qiao, S., and Sun, J., "A new approach for medical image enhancement based on luminance-level modulation and gradient modulation," *Biomedical Signal Processing and Control* **48**, 189–196 (2019).